Conference paper

Bianca Maranescu, Lavinia Lupa, Milica Tara-Lunga Mihali, Nicoleta Plesu, Valentin Maranescu and Aurelia Visa*

The corrosion inhibitor behavior of iron in saline solution by the action of magnesium carboxyphosphonate

https://doi.org/10.1515/pac-2018-0513

Abstract: Herein, we report the synthesis, structural characterization and corrosion assay of a metal phosphonate – $Mg(GLY)(H_2O)_2$ obtained from a tridentate ligand N,N-bis-phosphonomethylglycine (GLY) and a magnesium salt ($MgSO_4 \cdot 7H_2O$). The phosphonate was obtained by hydrothermal method at 80 °C and also under ultrasounds conditions at 60 °C. The FTIR, X-ray powder diffraction, elemental analysis and thermogravimetric analysis were performed in order to fully characterize the synthesized compounds and polarization experiments (CP) and electrochemical spectroscopy (EIS) to investigate the corrosion inhibition properties. The FTIR confirm the formation of magnesium phosphonate, and the X-ray diffraction showed the formation of a semi-crystalline compound. The elemental analysis confirmed the number of water molecules per formula unit of $Mg(HO_3PCH_2)_2N(H)CH_2COO \cdot 2H_2O$. The presence of nitrogen atom and phosphonate groups in the metal phosphonate structure anticipated that the presence of the small quantity of $Mg(GLY)(H_2O)_2$ in saline solution will provide a positive effect on iron surface and act as a corrosion inhibitor. From the CP curves recorded in an aerated nitric saline solution, corrosion parameters (corrosion potential –Ecorr, corrosion density current – Jcorr, polarization resistance – Rp and corrosion rate – Rcorr) were extracted from Tafel plots. The decrease in Jcorr is associated with a shift in Ecorr to more negative values. These results suggest that metal phosphonate behaves as a mixed-type inhibitor, by reducing both the cathodic and anodic reactions. The optimum inhibitor concentration determined was 2 mM. At this concentration the corrosion rate decreases by 23 % fold comparatively with iron in nitric acid solution without metal phosphonate. The EIS data in agreement with the polarization measurement resulted from polarization data.

Keyword: corrosion protection; ICGC-7; metal phosphonates.

Introduction

Mild steel is an excellent material widely used in industry due to its mechanical properties and low cost. Corrosion, deterioration of metal, in water or acidic systems affects the environment; therefore, to protect

Article note: A collection of invited papers based on presentations at the 7th International IUPAC Conference on Green Chemistry (ICGC-7), Moscow, Russia, 2–5 October 2017.

***Corresponding author: Aurelia Visa,** Institute of Chemistry Timisoara of the Romanian Academy, Timisoara, Romania, e-mail: apascariu@yahoo.com
Bianca Maranescu, Milica Tara-Lunga Mihali and Nicoleta Plesu: Institute of Chemistry Timisoara of the Romanian Academy, Timisoara, Romania
Lavinia Lupa: Politehnica University of Timisoara, Faculty of Industrial Chemistry and Environmental Engineering, Timisoara, Romania
Valentin Maranescu: Politehnica University of Timisoara, Faculty of Electronics and Telecommunications, Timisoara, Romania

metals against dissolution by corrosion it is very important to use the suitable inhibitors [1]. Inhibitors, even in very small concentrations, can efficiently reduce the corrosion rate. Donor–acceptor interaction between the metal and inhibitor forms a thin protective film on the metal surface that reduces the corrosion rate.

Phosphonates, due to their properties: low toxicity, high hydrolysis stability, adsorption on the metal surface, cannot be easily degraded by microorganisms, and corrosion inhibition activity in neutral aqueous media has been used as water treatment agents [2, 3]. Several research groups have carried out corrosion inhibition studies using phosphonic acids and carboxyphosphonic acids [4–12].

In phosphonate based inhibitor system, the inhibition efficiency was increased by the addition of divalent and trivalent metal. In the above study magnesium was chosen as metal ion to enhance the inhibition property of phosphonate.

Interest has been focused on designing chemical synthesis of new metal phosphonates to cover many application areas such as sensors, corrosion assay materials, electro-optics, filtration, ion exchange, catalysts [13–15]. Since hydrothermal reactions typically require up to several days, it is essential to develop easily, rapidly, commercially feasible routes to the production of these compounds. The ultrasonic synthesis method has attracted growing attention for the synthesis of nanomaterials [16–21]. We used two hydrothermal synthesis methods for preparation of metal phosphonate in water bath and ultrasonic synthesis.

Metallic surfaces open to air are usually covered with oxide film, which limits spontaneous degradation. When the metal is immersed in an aqueous solution, the oxide film is inclined to dissolve. The corrosion of mild steel in acid and saline ambiance remains in attention of scientists due to the protection necessity of metal surfaces from processed products: oil, gas and/or chemicals and transportation [22]. The presence of corrosion-inducing species in solution such as nitrate and chloride may interfere with the anodic passivation and undergo iron dissolution.

A number of organic substances containing nitrogen, oxygen, sulfur or phosphorous atoms and/or aromatic rings make possible their adsorption on the metal surface compounds and present effective inhibition for the corrosion of steel in acidic and saline environments [23, 24]. In general, the predisposition to form a stronger coordination bond, and as a result to present high inhibition efficiency, increases in the following order: O < N < S < P [25]. Compounds with a phosphonic functional group are effective chemicals capable to restrain the corrosion process [12, 26].

Herein, we report the synthesis, structural characterization and corrosion assay $Mg(GLY)(H_2O)_2$ – magnesium phosphonate metal organic framework.

Experimental

Materials and methods

All chemicals were obtained from commercial sources and used without further purification, except the bidistilled water. The reagents were stirred briefly, and the pH was measured before heating. The pHs were measured using a pH HI 2221 Calibration Check pH/ORP Meter by Hanna Instruments.

The crystallinity of the samples was examined using X-ray diffraction (XRD) analysis with Cu K_α radiation (PANalytical X'Pert Pro MPD diffractometer equipped with PixCel detector and spinning sample holder, working parameters 45 kV and 30 mA).

Carbon and hydrogen elemental composition of the compounds were performed using an automatic analyzers with CE-440 Elemental Analyzer, Exeter Analytical Inc., while phosphorus elemental analysis was determined by modified Schöniger method [27].

FT-IR spectra were recorded on a Jasco-FT/IR-4200 instrument in the range 400–4000 cm^{-1} on compressed KBr pellets. Attenuated Total Reflectance Infrared (ATR-IR) spectra were recorded with a FT/IR-4200 JASCO Spectrophotometer, equipped with PIKe ATR (MIRacle), DTGS detector, Ge crystal plate. These experiments were set at a resolution of 4 cm^{-1} in the range of 4000–600 cm^{-1}. All data were analyzed by the Spectral

Manager Version 2 software. The thermal stability of the materials was monitored between 30 and 700 °C under a flow of air or N_2 with a heating rate of 10 °C/min, using a Perkin Elmer Diamond thermogravimetric analyzer. The surface morphologies of the iron electrode in nitric saline medium in presence and absence of different concentrations of inhibitor were examined using a ZEISS STEMI 508 microscope.

For ultrasound synthesis was used an ELMA Hans Schmidbauer GmbH & Co. KG ultrasound bath, ELMASONIC ELMA S 10H model.

Synthesis of $Mg(GLY)(H_2O)_2$

A 100 mL round-bottomed flask was charged with $MgSO_4{\cdot}7H_2O$ (100.0 mmol), N,N-bis(phosphonomethyl) glycine (100.0 mmol), urea (100.0 mmol), and distilled water (100 mL). The pH was adjusted to 2.8 with an aqueous solution of NaOH (0.1 M). The mixture was divided in two equal parts and allows reacting in two alternative routes. The solution was heated in an oil-bath at 80 °C for 75 h. The reactant solution was heated in a ultrasound bath at 60 °C for 20 h. The resulting crystals were collected by filtration, washed with distilled water and dried in air (yield: 68 % on oil-bath, 32 % on ultrasound, respectively) [28–30].

The synthesized compounds were characterized by FTIR, X-ray crystallography powder diffraction, elemental analysis and thermogravimetric analysis.

Corrosion inhibitor studies

Corrosion assay regarding inhibitory effect of $Mg(GLY)(H_2O)_2$, electrochemical tests were performed in a Dcorr corrosion cell using Autolab 302N EcoChemie. The concentrations of the inhibitor were varied from 2.0 to 10.0 mM $Mg(GLY)(H_2O)_2$. The metal phosphonate is dissolved in dilute nitric acid saline solution (0.014 M HNO_3). The diluted nitric acid saline solution was prepared using nitric acid (Merck, 65 %) and saline water (3 % NaCl). The diluted nitric acid saline solution in the absence of $Mg(GLY)(H_2O)_2$ was use as a blank. The working electrode presents an exposed area of 0.785 cm^2, two stainless steel bars and Ag/AgCl were used as counter electrodes and reference electrode, respectively. The open-circuit potential (OCP) variation in time and the polarization curves (obtained by scanning the potential of iron from –1200 to 200 mV at a scan rate of 1 mV/s) were recorded in an aerated saline solution contain 0.035 M HNO_3 and 3 % NaCl. Corrosion parameters (corrosion potential –Ecorr, corrosion density current – Jcorr, polarization resistance – Rp and corrosion rate – Rcorr) were extracted from Tafel plots. EIS measurements were conducted around OCP values, at 22 ± 1 °C under potentiostatic mode. The impedance data was modelled by an equivalent electric circuit. Complex nonlinear simulation was performed used for simulation the program Zview – Associated Scribner Inc. and Levenberg – Marquard procedure [31].

Results and discussion

Best results both on yield and crystallinity was observed for the synthesis performed on the water bath method. Therefore, the analysis listed below are presented for $Mg(HO_3PCH_2)_2N(H)(CH_2COO)(H_2O)_2$ sample obtained in this method.

FTIR spectra of $Mg(GLY)(H_2O)_2$ and free ligand compounds are given in Fig. 1a. The free ligand contains the characteristic groups for carboxylate and phosphonate. The spectrum presents intense bands between 900 and 1200 cm^{-1}, which corresponds to the $–PO_3$ stretching vibration of GLY and one band at 1732 cm^{-1}, which corresponds to the asymmetric $\nu_{as}(C{=}O)$ stretch of uncoordinated carboxylic acids. FTIR spectra of $Mg(GLY)(H_2O)_2$ show a broad band at 3320 cm^{-1} assigned to Mg-coordinated water molecules, the $\nu_{as}(C{=}O)$ has shifted to 1612 cm^{-1} and the region 900 – 1200 cm^{-1} is rich in bands, which are mainly assigned to the phosphonate moieties. The decrease of the peak in the region 2500–2700 cm^{-1} attributed to P–OH vibrations confirms the formation on $Mg(HO_3PCH_2)_2N(H)(CH_2COO)(H_2O)_2$ compound.

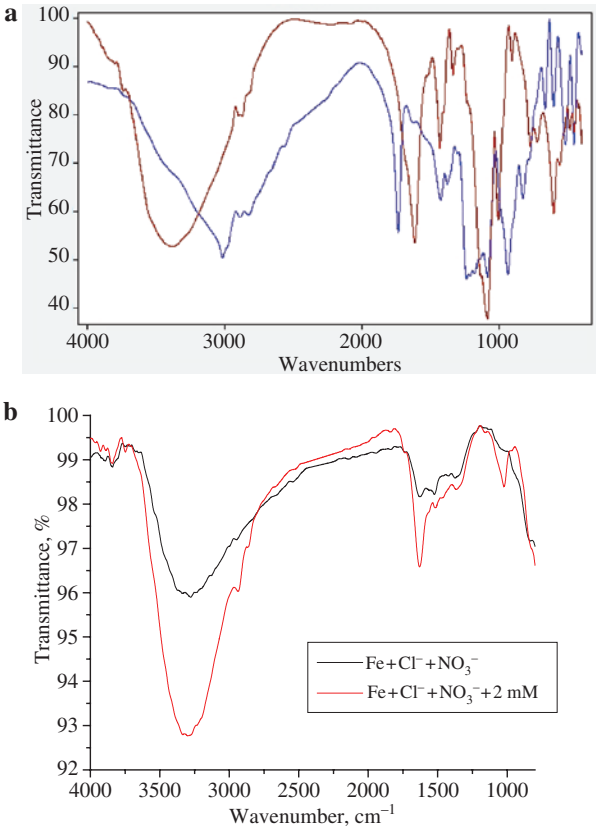

Fig. 1: FTIR spectra of (a) Mg(GLY)$(H_2O)_2$ red spectrum and GLY-free ligand blue spectrum and (b) ATR-FTIR spectra of layer deposited on iron surface after 1 h immersion in nitric saline solution and 2 mM inhibitor.

The sample showed the characteristic of a semi-crystalline solid, judging from the intensity and broad diffraction peaks in the 2θ region (Fig. 2).

Elemental analysis confirmed the number of water molecules per formula unit. $Mg(HO_3PCH_2)_2N(H)CH_2COO \cdot 2\ H_2O$ (M = 321.4 g/mol): calcd: C, 14.97 %; P, 19.27 %; H 4.01 %; Mg, 7.56 % found: C, 15.07 %; P, 20.54 %; H, 3.51 %; Mg, 7.02 %.

In order to determine the thermal stability of Mg(GLY)$(H_2O)_2$ thermogravimetric analysis (TGA) on crystalline samples were carried out in the presence of nitrogen atmosphere. Thermogravimetric analysis for

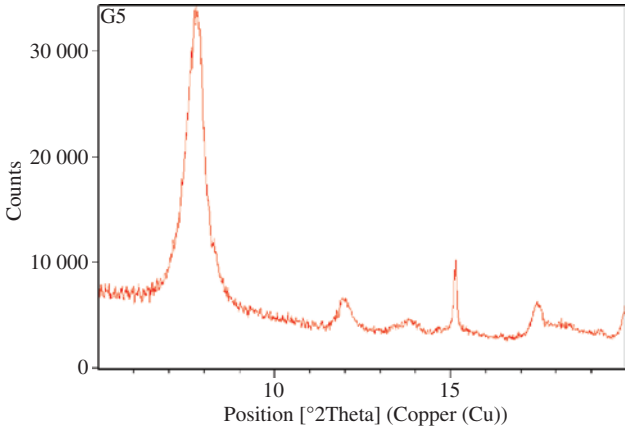

Fig. 2: X-ray pattern of Mg(GLY)$(H_2O)_2$.

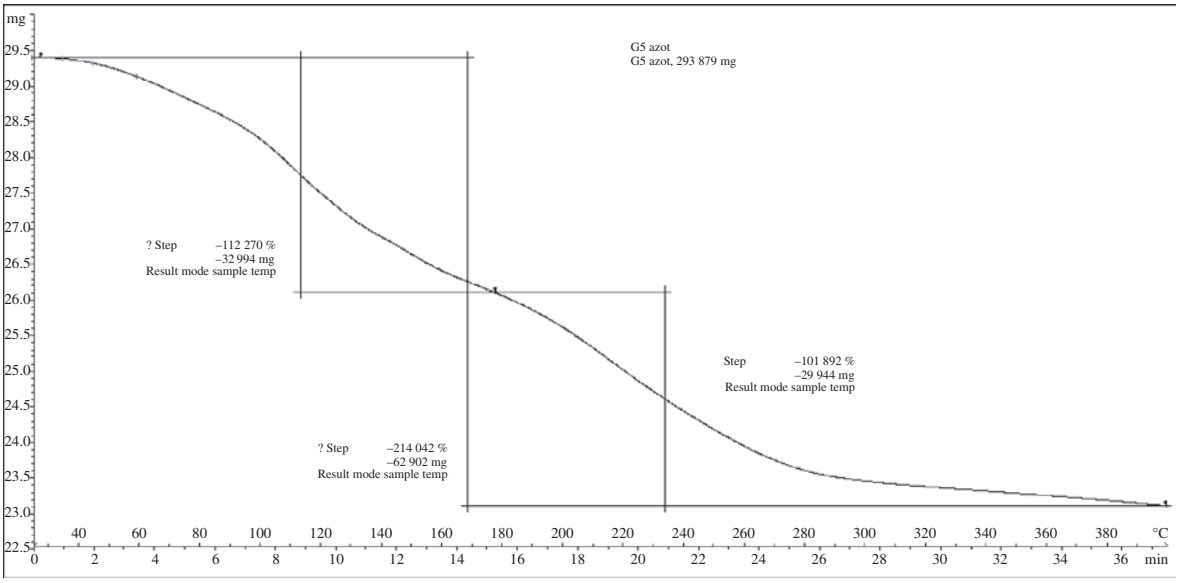

Fig. 3: Thermal behavior of $Mg(GLY)(H_2O)_2$ at 10 °C/min heating rate.

$Mg(GLY)(H_2O)_2$ (Fig. 3) confirms the crystallization of the solid with crystallization water. The DTA-TG curves only show distinct mass losses: one mass loss at 70–120 °C which indicates the loss of one water molecule coordinated to magnesium ion and the second process at 140–260 °C which is due to release of the second water molecule. Above this temperature the thermal decomposition of non-hydrated Mg(GLY) initiates.

Our obtained results are preliminary and opened up outlook to find a protocol for ultrasound synthesis varying the temperature, pH and ultrasonation time.

$Mg(GLY)(H_2O)_2$ material have a flower-like morphology and can be observed from the SEM images presented in Fig. 4. Each flower-like $Mg(GLY)(H_2O)_2$ consists of layer-shaped particle.

The donor–acceptor interaction between metal and inhibitor provides a thin protective layer as a result of chemisorption binding on the metal surface, capable to diminish the corrosion rate. The presence of nitrogen atom and phosphonate groups it is expected that the presence of the small quantity of $Mg(GLY)(H_2O)_2$ in dilute nitric acid saline solution had a positive effect on the passivation of iron and the compound behave as a corrosion inhibitor. Usually an inhibitor dispersed in the solution reduces the metal corrosion by blocking and/or electrocatalytic action. This type of compounds offer some advantages as: continuous 2D and 3D structure, topologies rich in π-systems or functional groups and hetero-aromatic moieties and recommends these compounds as potential materials for corrosion inhibition. The adsorption of the investigated inhibitor can be attributed to the presence of nitrogen atoms or can also occur through interactions between the carboxylate and P–OH groups and the iron surface. The optical images recorded on iron surfaces immersed in nitric saline solution without inhibitor revealed general corrosion. The presence of $Mg(GLY)(H_2O)_2$ in solution generates a protective coating on the surface observed in Fig. 4d and f. The surface of iron electrodes in solution without inhibitor, Fig. 4c and e, shows a corroded surface. These optical images validate the corrosion protection ability of this kind of compounds.

ATR-FTIR spectroscopy was used as tool for examination of layer formed on iron surface after immersion in nitric saline solution with inhibitor. Because the iron electrodes were well washed prior to analysis, it can be assumed that the inhibitor is grafted to the iron surface and not simply physisorbed. The ATR-FTIR data indicate that the inhibitor is present in the metal surface (is grafted to the iron surface and not simply by physical sorption). In organophosphorus layer deposited on iron surface, bands at 1343 cm^{-1} and 1023 cm^{-1} associated with P=O and P–O–C bonds was observed. The shoulders at 988 cm^{-1}, 965 cm^{-1} and 947 cm^{-1} correspond to the P–OFe and/or P–OH vibration [32] as a result of MgGLY binding to iron surface. In the spectrum of iron immersed in nitric saline solution with inhibitor the absence of the C=O stretching band characteristic

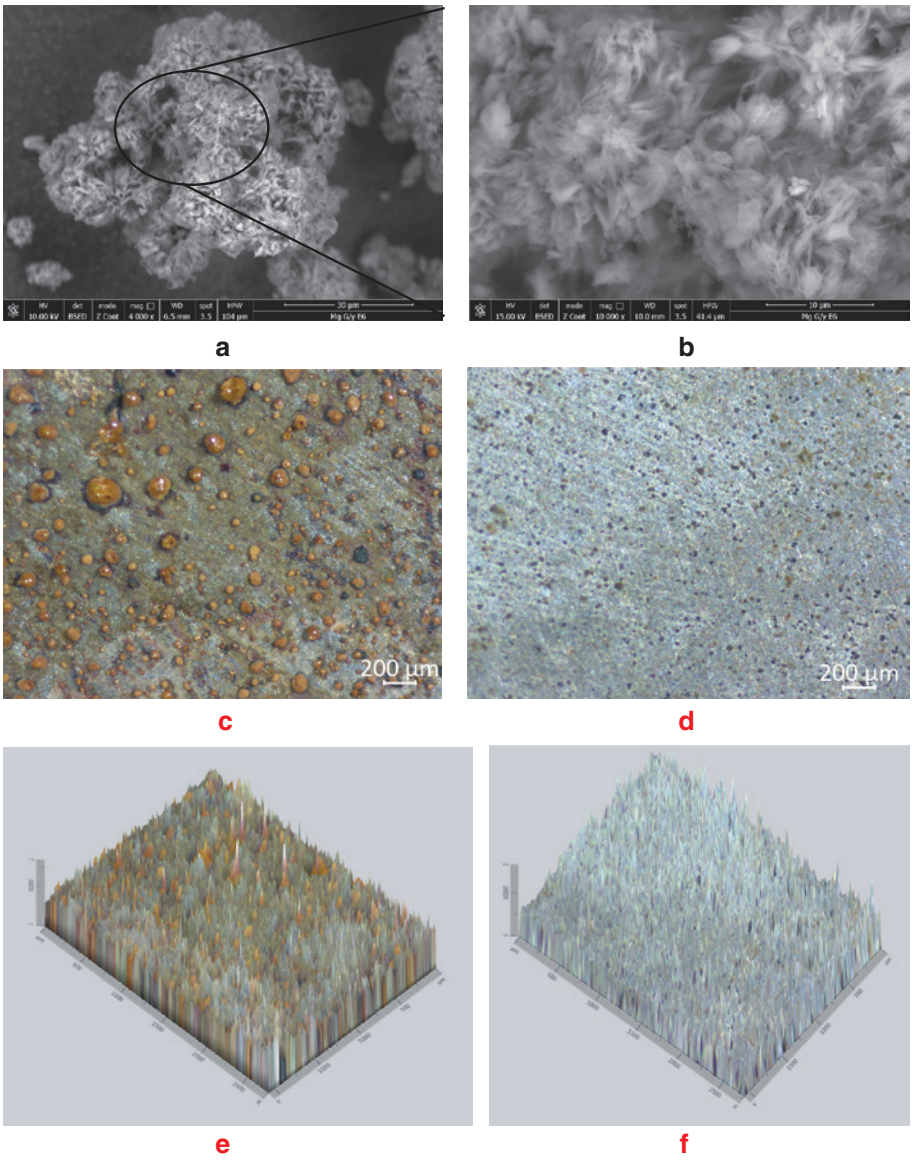

Fig. 4: Low magnification SEM images of $Mg(GLY)(H_2O)_2$ (a) medium magnification image flower like (b), optical images for no inhibitor (c) and with inhibitor (d) 2D optical images for no inhibitor (e) and with inhibitor (f) of iron electrodes after exposure for one 48 h to nitric saline solution.

of the COOH group at ~1710 cm^{-1} indicates that inhibitor is bonded to the iron surface through the carboxylate group (Fig. 1b). The asymmetric stretching C=O band appear to 1520 cm^{-1} and was shifted due to the metal coordinated carboxylates [33, 34]. The methylene group bands appear at 1420 cm^{-1} and 2847 cm^{-1} and 2931 cm^{-1}, respectively. The bands for N–H appear at 1625 cm^{-1} and 3410 cm^{-1}. The absence of the band at 2550 cm^{-1} pointed to a binding mode mostly through P–O–Fe bonds to the iron surface. The broad band at ~3300 cm^{-1} was attributed to OH stretching vibrations and overlap with the band for N–H.

The variation of OCP potential in time is presented in Fig. 5. It was observed that the OCP value for iron immersed in chlorine solution decreased in time after 60 s as a result of dissolution of passive oxide layer formed at the sample surface (electrodes), explained by the harsh chloride ions attack. For iron immersed in dilute nitric acid in time, a partially protection of surface took place by forming corrosion species capable to block the existing pores and cracks from the sample surface and conducting to potential stabilization. For the stabilization of OCP longer time is needed.

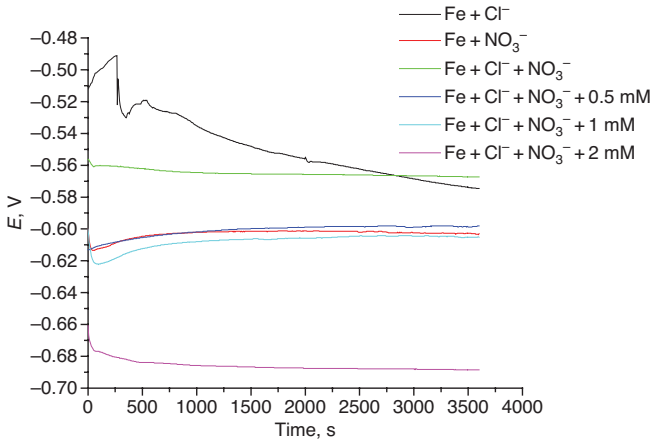

Fig. 5: The variation of OCP potential in time for iron immersed in: 3 % NaCl solution (black), 0.035 M HNO_3 solution (red), 3 % NaCl solution and 0.035 M HNO_3 solution (green), 3 % NaCl solution and 0.035 M HNO_3 solution with 0.5 mM inhibitor (blue) and 3 % NaCl solution, 0.035 M HNO_3 solution with 0.5 mM inhibitor (cyan) and 3 % NaCl solution and 0.035 M HNO_3 solution with 2 mM inhibitor (magenta).

In acidic solution, chloride ions participate in the process of anodic metal dissolution probably through their adsorption on the metal surface forming activated intermediates ($FeOH^+$ or $FeCl^+$ad) which will determine the metal dissolution [35]. In nitric acid solution the Fe is oxidized to $Fe(OH)_2$ and then to Fe_3O_4 by nitrate. As nitrite is formed in solution nitrate is reduced and the Fe_3O_4 might be oxidized to FeOOH or Fe_2O_3, which are more stable compounds.

The OCP of iron in nitric acid and saline solutions containing $Mg(GLY)(H_2O)_2$ reaches the steady-state value faster than in saline solutions. Furthermore, the steady-state values of OCPs in nitric acid and saline solutions containing metal phosphonate present fewer oscillations than in the saline solution. This suggests that the inhibition effect mainly depends on the adsorption amount of metal phosphonate on metal surface which is linked to the amount of metal phosphonate present in solution. It is also clear that by increasing metal phosphonate concentration, the inhibition efficiency increased due to the increased amount of metal phosphonate adsorbed on metal surface and the formation of dense adsorbed layer with a high corrosion protection effect. It was concluded that the mechanism of inhibition was anodic type, hindering active iron dissolution due to the blocking of the metal surface.

From the polarization curves after 90 min immersion, the corrosion density current and corrosion rate were determined from extrapolation of Tafel plots (Fig. 6) and values are presented in Table 1.

The polarization resistance calculated from Tafel plots indicate 10 times higher value for iron immersed in 2 mM inhibitor, suggesting a good adsorbed layer of inhibitor on metallic surface. At inhibitor concentration in solution lower than 2 mM the adsorbed layer seems to be insufficient and susceptible for aggressive attach. Corrosion resistance Rcorr is lower for iron immersed in 2 mM inhibitor, suggesting also a good adsorbed layer of inhibitor on metallic surface at this concentration. The corrosion density Jcorr, of iron in nitric acid solution without inhibitor is 6.27×10^{-5} A · cm^{-2}. It was observed that the values of Jcorr decreases with increasing of metal phosphonate concentration from 3.435×10^{-5} A · cm^{-2} at 1 mM to 2.778×10^{-6} A · cm^{-2} at 2 mM. The decrease in Jcorr is associated with a shift in Ecorr to more negative values. These results suggest that metalphosphonate behaves as a mixed-type inhibitor, by reducing both the cathodic and anodic reactions. These results indicate that the anodic and cathodic branches related to the dissolution of the iron and oxygen reduction respectively weakened the corrosion process. The effect on cathodic reaction is more obvious. This metal phosphonate presents an inhibition effect upon corrosion in aggressive media. In literature phosphonate compounds were reported to be mixed inhibitors [36].

In Fig. 7 the impedance spectra Nyquist graph (Fig. 7a) shows the imaginary component of the impedance plotted as a function of the real component, and the Bode representation (Fig. 7b) shows the logarithm of the impedance modulus |Z| and phase angle as a function of the logarithm of the frequency f.

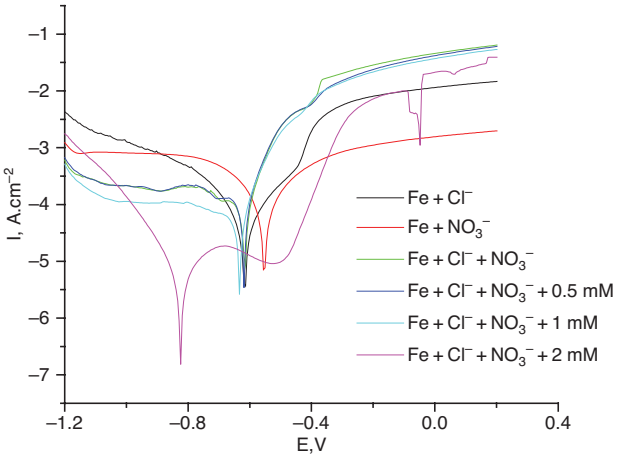

Fig. 6: Polarization curves for 3 % NaCl solution (black), 0.014 M HNO_3 solution (red), 3 % NaCl solution and 0.014 M HNO_3 solution (green), 3 % NaCl solution and 0.014 M HNO_3 solution with 0.5 mM inhibitor (blue) 1 mM inhibitor (cyan) and 3 % NaCl solution and 0.035 M HNO_3 solution with 2 mM inhibitor (magenta).

Table 1: Electrochemical parameters for iron after 90 min immersion in 0.014 M HNO_3 and 3.0 wt % NaCl solutions with and without inhibitor.

Sample	Jcorr, A/cm²	bc, V/decade	ba, V/decade	Rp, Ω	Ecorr, Ω	Rcorr. mm/year
Fe-Cl	2.610×10^{-5}	0.078	0.057	120.1	−0.61	0.296
Fe-NO_3	5.688×10^{-5}	0.110	0.086	91.7	−0.55	0.817
Fe-NO_3-Cl	6.270×10^{-5}	0.120	0.105	110.2	−0.55	0.901
Fe-NO_3-Cl + 0.5 mM	6.080×10^{-5}	0.152	0.512	49.02	−0.61	0.874
Fe-NO_3-Cl + 1 mM	3.438×10^{-5}	0.131	0.053	112.4	−0.63	0.494
Fe-NO_3-Cl + 2 mM	2.778×10^{-6}	0.054	0.099	1067	−0.83	0.039

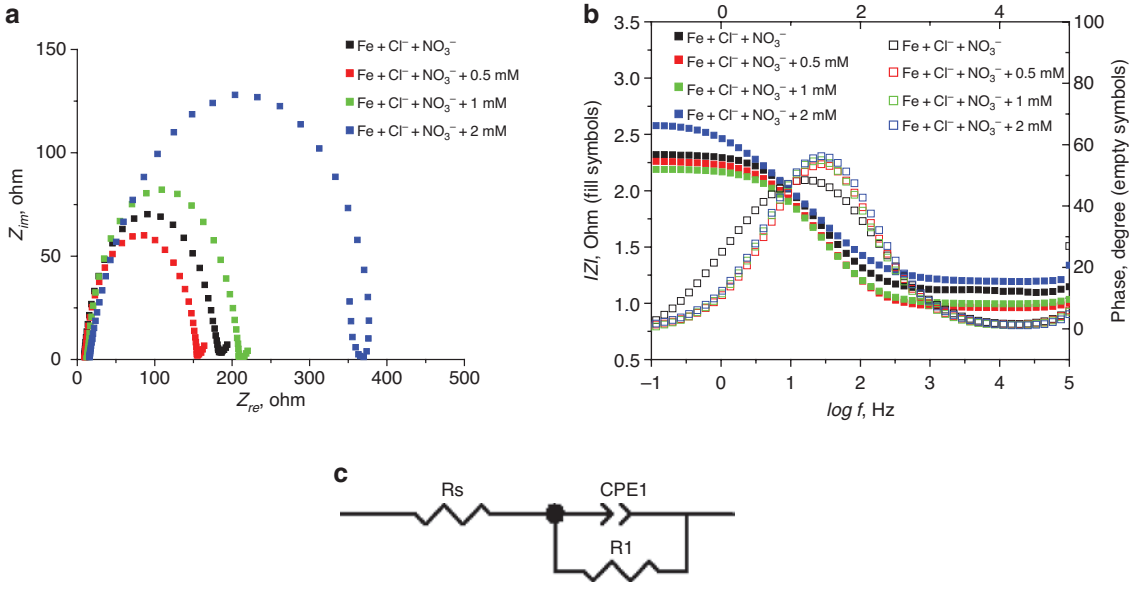

Fig. 7: Impedance spectra (a) Nyquist graph, (b) Bode representation (logarithm of the impedance modulus |Z| (fill symbols) and phase angle (hollow symbols) as a function of the logarithm of the frequency f, recorded in 0.014 M HNO_3 with 3 % NaCl solution and (c) schematic representation of the electric equivalent circuit for EIS data.

Table 2: The value of EIS parameters.

Specimen	χ^2	Sum-Sqr	Rs(+)	Q-T $F \cdot cm^{-2}$	Q-P, (ϕ)	R1 $\Omega \cdot cm^2$
Fe-NO_3-Cl	4.78×10^{-03}	0.55	9.176	2.72×10^{-04}	0.89	174.10
Fe-NO_3-Cl + 0.5 mM	5.50×10^{-03}	0.64	9.932	2.81×10^{-04}	0.89	146.10
Fe-NO_3-Cl + 1 mM	5.09×10^{-03}	0.59	12.93	2.24×10^{-04}	0.89	198.00
Fe-NO_3-Cl + 2 mM	3.90×10^{-02}	4.53	15.89	3.84×10^{-04}	0.78	359.90

The complex plane (Nyquist) plots (Fig. 7a) show a higher capacitive semicircle for iron immersed in solution containing inhibitor, which indicates that the metal phosphonate is adsorbed on the metal surface and presents the highest total impedance and the highest corrosion resistance, in agreement with the polarization measurement results from polarization data.

Figure 7b shows the Bode plots and shows one time constant link with the corrosion process. A simple Randler circuit (Fig. 7c) containing only the resistance of electrolyte Rs, the resistance R1 and double layer capacitance CPE1 was used for modelled EIS.

Constant phase element (CPE) was bringing in to represent the double layer capacitance and for the reason of non-ideal behaviour the impedance of a CPE was used, expressed by $Z_{CPE} = [T(j\omega)^n]^{-1}$, where ω is frequency; T is the CPE magnitude and the exponent n is between 0 and 1. The values of EIS parameters for samples are presented in Table 2.

The R1 value depends on the degree of inhibitor molecules to be adsorbed on metal surface. Gradual replacement of water molecules on the metal surface takes place with the adsorption of inhibitor and the formation of inhibitor layer on metal surface. This will decrease the amount of metal dissolution and reduce the corrosion rate. It was observed that the R1 increase with the increase of inhibitor concentration. The value of R1 is a measure of quality of protective layer of adsorbed molecules at metal surface; a higher value indicates a good protection and describes the ability of the coating to hold down ion transfer at the solution/coating interface. The surface of iron immersed in the solution containing 2 mM inhibitor shows time constant at a lower frequency value and a higher module of impedance and points out to a better barrier performance. The lower value for R1 (polarization resistance) obtained from EIS data for iron immersed in solution without or with inhibitor lower than 2 mM show low protective barrier (porous and thicker layer) and the aggressive solution could directly infiltrate to the metal surface and initiate the corrosion process. At 2 mM inhibitor concentration in solution the R1 is highest due to the increased adsorbed number of molecules on metal surface able to offer proper protection against corrosion, which meant that metal phosphonate had ability to form a protective film on the metal surface.

The impedance data for coated sample are correlated well to polarization data.

Conclusions

In summary, we reported the synthesis and structural characterization of the 2D coordination polymer $Mg(GLY)(H_2O)_2$ a phosphonate metal organic framework using two alternative synthetic routs. Organized studies can let to identify proper synthetic parameters in different synthetic conditions. The best crystallinity of the presented materials was observed in the reaction $MgSO_4 \cdot 7H_2O$ and N,N-bis(phosphonomethyl)glycine acid using hydrothermal condition at 80 °C.

The value for R1 corresponds to the resistance of coatings and increase with the coating thickness and decrease with the increase of pore number and size. R1 values increased with inhibitor concentration and reached maximum value at 2 mM.

Acknowledgments: This work was partially supported by Program no 2, Project no. 2.3 from the Institute of Chemistry Timisoara of Romanian Academy and by a grant of Ministery of Research and Innovation, CNCS – UEFISCDI, project number PN-III-P1-1.1-TE-2016-2008, within PNCDI III.

References

[1] H. S. Awad, S. Turgoose. *Corrosion* **60**, 116 (2004).
[2] A. M. Al-Sabagh, H. M. Abd-El-Bary, R. A. El-Ghazawy, M. R. Mishrif, B. M. Hussein. *Egypt. J. Petrol.* **20**, 33 (2011).
[3] S. Rajendran, B. V. Apparao, N. Palaniswamy. *Electrochim. Acta* **44**, 533 (1998).
[4] H. Amar, J. Benzakour, A. Derja, D. Villemin, B. Moreau, T. Braisaz, A. Tounsi. *Corros. Sci*. **50**, 124 (2008).
[5] H. Amar, J. Benzakour, A. Derja, D. Villemin, B. Moreau. *J. Electroanal. Chem*. **558**, 131 (2003).
[6] G. Gunasekaran, N. Palaniswamy, B. V. Apparao. *Bull. Electrochem*. **12**, 59 (1996).
[7] S. Rajendran, B. V. Apparao, N. Palaniswamy. *Anti Corros. Methods Mater.* **47**, 147 (2000).
[8] J. L. Fang, Y. Li, X. R. Ye, Z. W. Wang, Q. Liu. *Corrosion* **49**, 266 (1993).
[9] S. Rajendran, B. V. Apparao, N. Palaniswamy, V. Periasamy, G. Karthikeyan. *Corros. Sci.* **43**, 134513 (2001).
[10] D. Mohammedi, A. Benmoussa, C. Fiaud, E. M. M. Sutter. *Mater. Corros*. **55**, 837 (2004).
[11] M. Prabakaran, M. Venkatesh, S. Ramesh, V. Periasamy. *Appl. Surf. Sci.* **276**, 592 (2013).
[12] K. D. Demadis, C. Mantzaridis, P. Lykoudis. *Ind. Eng. Chem. Res*. **45**, 7795 (2006).
[13] K. J. Gagnon, H. P. Perry, A. Clearfield. *Chem Rev.* **112**, 1034 (2012).
[14] B. Maranescu, A. Visa, G. Ilia, Z. Simon, K. D. Demadis, R. M. P. Colodrero, A. Cabeza, O. Vallcorba, J. Rius, D. Choquesillo-Lazarte. *J. Coord. Chem*. **67**, 1562 (2014).
[15] A. Visa, M. Mracec, B. Maranescu, V. Maranescu, G. Ilia, A. Popa, M. Mracec. *Chem. Cent. J.* **6**, 91(2012).
[16] B. Zhang, A. Clearfield. *J. Am. Chem. Soc*. **119**, 2751 (1997).
[17] K. J. Gagnon, H. P. Perry, A. Clearfield. *Chem. Rev.* **112**, 1034 (2012).
[18] M. Bazaga-García, R. M. Colodrero, M. Papadaki, P. Garczarek, J. Zoń, P. Olivera-Pastor, E. R. Losilla, L. León-Reina, M. A. Aranda, D. Choquesillo-Lazarte, K. D. Demadis, A. Cabeza. *J. Am. Chem. Soc.* **136**, 5731 (2014).
[19] J. -G. Mao, Z. Wang, A. Clearfield. *New J. Chem*. **26**, 1010 (2002).
[20] W. -J. Son, J. Kim, W. -S. Ahn. *Chem. Commun.* **47**, 6336 (2008).
[21] L. -G. Qiu, Z. -Q. Li, Y. Wu, W. Wang, T. Xu, X. Jiang. *Chem. Commun*. **31**, 3642(2008).
[22] H. Keles, M. Keles. *Mater. Chem. Phys*. **112**, 173 (2008).
[23] R. Solmaz, G. Kardas, B. Yazicl, M. Erbil. *Colloids Surf. A: Physicochem. Eng. Aspects* **312**, 7 (2008).
[24] A. Popova, M. Christov, S. Raicheva, E. Sokolova. *Corros. Sci.* **46**, 1333 (2004).
[25] S. Sankarap, F. Apavinasam, M. Pushpanaden, F. Ahmed. *Corros. Sci.* **32**, 193 (1991).
[26] M. Prabakaran, M. Venkatesh, S. Ramesh, V. Periasamy. *Appl. Surf. Sci*. **276**, 592 (2013).
[27] A. Popa, V. Parvulescu, S. Iliescu, N. Plesu, G. Ilia, L. Macarie, A. Pascariu. *Plast. Rubber Compos*. **37**, 193 (2008).
[28] R. M. P. Colodrero, A. Cabeza, P. Olivera-Pastor, D. Choquesillo-Lazarte, A. Turner, G. Ilia, B. Maranescu, K. E. Papathanasiou, G. B. Hix, K. D. Demadis, M. G. Aranda. *Inorg. Chem.* **50**, 11202 (2011).
[29] O. Vallcorba, J. Rius, C. Frontera, C. Miravitlles. *J. Appl. Crystallogr*. **45**, 1270 (2012).
[30] K. D. Demadis, M. Papadaki, M. A. G. Aranda, A. Cabeza, P. Olivera-Pastor, Y. Sanakis. *Cryst. Growth Des*. **10**, 357 (2010).
[31] http://www.scribner.com/ Electrochemical Impedance Spectroscopy measurements.
[32] M. I. Tejedor-Tejedor, M. A. Anderson. *Langmuir* **6**, 602 (1990).
[33] L. J. Bellamy. *The Infrared Spectra of Complex Molecules*, Chapman and Hall, London (1975).
[34] K. D. Demadis, N. Famelis, A. Cabeza, M. A. G. Aranda, R. M. P. Colodrero, A. Infantes-Molinas. *Inorg. Chem*. **51**, 7889 (2012).
[35] N. Sato. *Corrosion* **45**, 354 (1989).
[36] M. Prabakaran, K. Vadivu, S. Ramesh, V. Periasamy. *Egypt. J. Petrol.* **23**, 367 (2014).